Agricultural Water Management 205 (2018) 63–71

Contents lists available at ScienceDirect

Agricultural Water Management

journal homepage: www.elsevier.com/locate/agwat

Impacts of climate change on soybean production under different treatments of field experiments considering the uncertainty of general circulation models

Hamidreza Ahmadzadeh Araji[a,*], Aimrun Wayayok[a,b], Alireza Massah Bavani[c], Ebrahim Amiri[d], Ahmad Fikri Abdullah[a], Jahanfar Daneshian[e], C.B.S. Teh[f]

[a] Department of Biological and Agricultural Engineering, Faculty of Engineering, Universiti Putra Malaysia, 43400, Serdang, Selangor Darul Ehsan, Malaysia
[b] Smart Farming Technology Research Centre (SFTRC), Faculty of Engineering, Universiti Putra Malaysia, 43400, Serdang, Selangor Darul Ehsan, Malaysia
[c] Department of Irrigation and Drainage Engineering, College of Abureyhan, University of Tehran, Iran
[d] Department of Water Engineering, Lahijan Branch, Islamic Azad University, Lahijan, Iran
[e] Seed and Plant Improvement Institute, Department of Oil Seed Crops, Karaj, Iran
[f] Department of Land Management, Faculty of Agriculture, Universiti Putra Malaysia, 43400, Serdang, Selangor Darul Ehsan, Malaysia

ARTICLE INFO

Keywords:
AquaCrop
Yield
Biomass
GCMs
Emission scenarios

ABSTRACT

Earth is faced with dramatic changes in the weather systems, which leads to climate change. Climate change affects water resources and crop production. In this study, five and seven general circulation models (GCMs) were respectively collected via the IPCC Fourth and Fifth Assessment Reports. Emission scenarios including B1, A1B, and A2 for AR4 and RCP2.6 and RCP8.5 for AR5 were applied to predict future climate change. The weighting method of mean observed temperature-precipitation (MOTP) was utilized to compute uncertainty related to different climate models. The scenario files made by ΔT and ΔP were applied to the downscaled model of LARS-WG to generate weighted multi-model ensemble means of temperature and precipitation for the period 2020–2039 centered on 2030s. These ensemble means were incorporated into the calibrated AquaCrop model to predict final yield and biomass. In this study, soybean data were applied for four different varieties under three irrigation treatments in field experiments carried out at Karaj Seed and Plant Improvement Institute in two successive years. However, the results of statistical analysis between the model output and observed data for all varieties and irrigation treatments in the calibration year (2010) and validation year (2011) were the same at the 95% confidence level. It is suggested that AquaCrop is a valid model to predict yield and biomass for the study area in the future. Furthermore, comparing future climatic variables to the historical period during the soybean growing season showed enhancement of these variables by the 2030s. The amplitude change of temperature was larger in AR5, whereas the amplitude change of precipitation and CO_2 were larger in AR4. The soybean yield and biomass increased for all treatments in the 2030 s with positive correlation with the climatic variables. The maximum temperature represented the most significant correlation with yield and biomass for almost all treatments. Finally, soybeans might achieve an optimal threshold temperature in the future, leading to yield increases in the 2030s.

1. Introduction

Most parts of Iran are located in arid and semi-arid areas of the world, and Iran's agricultural sectors are highly dependent on water resources and rainfall. The phenomenon of climate change will have consequences such as water scarcity, temperature increase, and high evapotranspiration, which lead to water stress during crop growing periods. Soybean (Glycine max) is a legume crop that is globally popular as an oil seed crop. This legume is a substantial protein source for human feeding and is useful for biofuel feedstock and animal food (Masuda and Goldsmith, 2009).

Crop simulation models, which predict crop yield and biomass (Bannayan et al., 2003), are applicable tools in climate change impacts studies. The AquaCrop model was developed by FAO as a practical model for prediction of attainable yield and biomass for many generic crops under water-limiting conditions. The factors that distinguish this model from other crop models are minimal input parameters and a better balance between simplicity, accuracy, and robustness (Raes

* Corresponding author.
E-mail address: hamid_araji@yahoo.com (H. Ahmadzadeh Araji).

https://doi.org/10.1016/j.agwat.2018.04.023
Received 17 January 2018; Received in revised form 15 April 2018; Accepted 17 April 2018

et al., 2009b; Steduto et al., 2009). The performance of the AquaCrop model to simulate yield response to water stress has been reported by researchers for other crops in different parts of the world, including, for example, teff (Araya et al., 2010), cotton (Farahani et al., 2009; García-Vila and Fereres, 2012; Heidariniya et al., 2012; Hussein et al., 2011), sunflower and potato (García-Vila and Fereres, 2012; Yuan et al., 2013); rice (Amiri et al., 2015), barley (Tavakoli et al., 2015), winter wheat (Heidariniya et al., 2012; Salemi et al., 2011) and wheat (Andarzian et al., 2011; Shrestha et al., 2013). Atmosphere-ocean general circulation models (AOGCMs) are capable of estimating future climate change, especially at globally and continental scales. These numerical models can depict a comprehensive three-dimensional representation of the climate system, illustrating dynamical and physical processes, their interactions, and feedbacks. These models can provide a regional estimation of changes in aerosol concentration and greenhouse gases and their impact on future climate (Randall et al., 2007; Ruosteenoja et al., 2003). The IPCC (Intergovernmental Panel on Climate Change) has published SRES scenarios to survey future developments in the global environment by considering production sources of greenhouse gases and aerosol emissions. Resulting storylines such as A2, A1B, and B1 are respectively the representatives of high, moderate, and low growth rate of future emission scenarios. These emission scenarios, with different technological, social, demographic, economic, and environmental developments in increasingly unalterable ways (IPCC-TGICA, 2007), represent the relationships between the forces driving aerosol emissions and greenhouse gases, especially yearly atmospheric CO_2 concentration and its development during the 21 st century on a global scale. As the climate models became more sophisticated, the latest generation of GCMs were developed by the IPCC in support of the Fifth Assessment Report (AR5) as the fifth phase of the Coupled Model Intercomparison Project (CMIP5). However, as a result of considering land use changes and external forcing such as solar and volcanic forcing at a finer resolution, models were more sophisticated in CMIP5 (Knutti and Sedláček, 2012). Furthermore, the new Representative Concentration Pathway (RCP) with time- and space-dependent trajectories of concentrations of greenhouse gases and other forcing agents are used in CMIP5 as a very low forcing level (RCP2.6), two medium stabilization scenarios (RCP4.5/RCP6) and one very high baseline emission scenario (RCP8.5) (van Vuuren et al., 2011).

Since soybean production plays an important role in Iran for the agricultural and industrial sectors, study of climate change impacts on this crop is important. Moreover, in climate change impacts studies, existing uncertainties should be taken into consideration to produce more accurate outputs. Studies have shown that among different uncertainties, GCM outputs have the most influence on output results (Massah Bavani, 2006; Minville et al., 2008; Prudhomme and Davies, 2007). Notwithstanding the existing studies that have conducted on climate change impacts on different systems along with mitigation and adaptation methods, most studies have concentrated on sensitivity analysis and system vulnerability to one or few climate change scenarios (Alexandrov and Genev, 2003; Brouyère and Dassargues, 2004; Fowler et al., 2004; Gellens and Roulin, 1998; Kamga, 2001; Yates and Strzepek, 1998). Therefore, this study aims to project the weighted multi-model ensemble means as an uncertainty analysis method by applying GCM outputs under three emission scenarios (B1, A1B, and A2) and two Representative Concentration Pathways (RCP2.6, and RCP8.5). Furthermore, although few studies have been done regarding calibration of the AquaCrop model for soybean in this specific area, there is a research gap in comparing different cultivar reactions to water stress. This study predicts future changes on final grain yield and biomass in the study area for the period 2020–2039 centered on 2030 s by considering uncertainty of GCM outputs.

2. Materials and methods

2.1. Study area and experimental treatments

The study area was located in an experimental field of the Karaj Seed and Plant Improvement Institute, Iran (35°47′N, 50°54′E). This area has a cold semi-arid climate with a temperate summer and semi cold winter. The data are derived from two experiments in 2010 and 2011, which were carried out using a completely randomized block design with three replications. The entire cultivated area of soybean was approximately 3750 m^2 for the two experimental years.

AquaCrop version 4.0 (Raes et al., 2012b) was calibrated for year 2010 and validated for year 2011. Four soybean varieties including L17 (V1), Williams*Hobbit (W*H) (V2), M9 (V3), and M7 (V4) were sown on June 27, 2010, and July 4, 2011. Based on genotypes with different length of growing days, the cultivation date varied between the first to third weeks of October. Therefore, July to October were considered the most important months for the length of the crop cycle.

The irrigation method was the furrow system, and water was siphoned at a rate of 0.2 L s^{-1} discharge to deliver water to every furrow. The irrigation period started the first day after sowing, and full irrigation was considered when the water reached to the end of furrow. To perform the irrigation treatments, the cumulative evaporation values from a class-A pan were measured every seven days as a criterion for estimation of applied irrigation amount. Irrigation treatments were defined as without water stress (I1), mild water stress (I2), and severe water stress (I3) by adjusting pan evaporation values to 50, 100, and 150 mm, respectively. Based on these values, irrigation intervals were determined in 7, 14, and 21 days that were respectively assigned to the treatments of (I1), (I2), and (I3). Based on total water input, the irrigation depth, which was applied in the model, was approximately equal to 35 mm for each interval. However, the water stress treatments were conducted after the appearance of five to seven trifoliate leaves. In other words, the irrigation periods for all treatments were the same to the control treatments until five to seven trifoliate leaves. After this growth stage, irrigation treatments were conducted with total applied irrigation amounts of 525 mm (I1), 350 mm (I2), 280 mm (I3) for L17 and W*H, and 455 mm (I1), 315 (I2), and 245 mm (I3) for M9 and M7. Moreover, these irrigation amounts from the calibration year were applied as inputs of AquaCrop for historical and projected future periods.

2.2. AquaCrop model

AquaCrop is a water-driven model designed by yield response in relation to water supply and agronomic practices by using soil water budgeting (Raes et al., 2009b). The specifications of the model including conceptual framework, underlying principles, and distinctive components are discussed by Steduto et al. (2009), whereas the model algorithms and structural detail are described by Raes et al. (2009b). The fundamental equation, propounded by Doorenbos and Kassam in 1979, is shown in Eq. (1) as a basic equation for prognostication of yield response to water (Raes et al., 2009a):

$$\left(\frac{Y_x - Y_a}{Y_x}\right) = k_y\left(\frac{ET_x - ET_a}{ET_x}\right) \quad (1)$$

where Y_x and Y_a are the maximum and actual yield, ET_x and ET_a are the maximum and actual evapotranspiration, and k_y is the proportionality factor between relative yield loss and relative reduction in evapotranspiration.

2.2.1. Input data in the AquaCrop model

Input data, including weather, crop, soil, and field management data, define the crop development environment. Meanwhile, the crop input, as applied to the AquaCrop model, is determined from

Table 1
Input data of crop parameters used in the AquaCrop model.

Description	Values				Units	Remarks
	L17	W*H	M9	M7		
Base temperature	5.0	5.0	5.0	5.0	(°C)	D
Upper temperature	30.0	30.0	30.0	30.0	(°C)	D
Canopy growth coefficient (CGC)	0.25	0.25	0.25	0.25	% day^{-1}	D
Maximum canopy cover (CCx)	0.95	0.93	0.95	0.95	%	C
Canopy decline coefficient (CDC)	0.17	0.16	0.16	0.16	% day^{-1}	C
Water Productivity normalized	16	15.0	16.0	16.0	g m^{-2}	C
Soil water depletion factor for canopy expansion – Upper threshold	0.15	0.15	0.15	0.25	–	C
Soil water depletion factor for canopy expansion – Lower threshold	0.65	0.65	0.65	0.65	–	D
Shape factor for water stress coefficient for canopy expansion	3.0	3.0	3.0	3.0	–	D
Soil water depletion fraction for stomatal control – Upper threshold	0.50	0.50	0.50	0.25	–	C
Shape factor for water stress coefficient for stomatal control	3.0	3.0	3.0	3.0	–	D
Soil water depletion factor for canopy senescence – Upper threshold	0.70	0.70	0.70	0.75	–	
Shape factor for water stress coefficient for canopy senescence	3.0	3.0	3.0	3.0	–	D
Minimum effective rooting depth	0.30	0.30	0.30	0.30	m	D
Maximum effective rooting depth	0.60	0.60	0.60	0.60	m	D
Days from sowing to emergence	7	7	7	**7**	days	M
Days from sowing to start senescence	85	86	78	78	days	M
Days from sowing to maturity (length of crop cycle)	106	107	98	98	days	M
Days from sowing to flowering	35	34	33	33	days	M
Length of the flowering stage	22	22	22	22	days	M
Building up of HI starting at flowering	71	72	65	65	days	C
Reference harvest index (HI_0)	29	29	29	32	%	C

C – calibrated, D – default, M – measured.

experimental data, model defaults and calibrated parameters.

Climatic data such as maximum and minimum temperature and precipitation on a daily basis were collected from the Karaj meteorology station, which is less than four km away from the experimental field. The ETo calculation method, with Hargreaves–Samani (HS) as a temperature-based method, was chosen for decrement of uncertainties of climatic input. Moreover, the HS method is a suitable ETo estimation method for all climatic regions of Iran (Raziei and Pereira, 2013). The HS method is also known as one of the most precise models under semi-arid climatic conditions such as those of the study area (Tabari, 2010). The default mean annual atmospheric CO_2 concentration that was measured at the Mauna Loa observatory in Hawaii was used (Mustafa et al., 2017; Yang et al., 2017). Moreover, for future prediction, the emission scenarios and RCPs were selected from IPCC data that were available in the AquaCrop database. The input data of crop parameters and the measured physical soil characteristics for the study area are shown in Tables 1 and 2.

2.2.2. Model prediction accuracy

Model prediction accuracy evaluated based on most important statistical indicators including absolute root mean square error (RMSE) and root mean square error normalized (RMSEn). These indicators represented agreement between the observed and simulated final biomass and grain yield. The root mean square error (RMSE), which is the most practical statistical index used by crop modeling studies (Jacovides and Kontoyiannis, 1995), ranges from 0 to positive infinity. As residual estimation errors decrease, the RMSE values are close to zero. The mean square error normalized (RMSEn) is on a percentage scale and is an indicator for displaying relative differences between predictions and observations. Raes et al. (2012a) declared that values of RMSEn are excellent if smaller than 10%, good if between 10 and 20%, fair if between 20 and 30% and poor if larger than 30%. The mean bias error (MBE) reveals the long-term performance of the model. A positive value of the MBE gives the average amount of overestimation in the estimated values and vice versa (Iqbal et al., 2014).

Table 2
Soil physical characteristics of sandy loam soil in the experimental fields.

Soil texture	Permanent wilting point (PWP) (vol %)	Field capacity (FC) (vol %)	Saturation point (SAT) (vol %)	Total available water (TAW) (mm/m)	Saturated hydraulic conductivity (Ksat) (mm/day)
Sandy loam	13.0	24.0	46.0	110	380.0

The Eqs. (2)–(4) are the equations of (RMSE), (RMSEn), and (MBE) respectively.

$$RMSE = \left[\frac{\sum_{i=1}^{n} (Pi - Oi)^2}{n} \right]^{1/2} \quad (2)$$

$$RMSEn = 100 \frac{RMSE}{Omean} \quad (3)$$

$$MBE = \frac{1}{n} \left[\sum_{i=1}^{n} Pi - Oi \right] \quad (4)$$

where P_i and O_i is the simulated and observed value, respectively, O_{mean} is the mean observed data, and n is the number of measurements. The "goodness-of-fit" between the observed and simulated yield and biomass was assessed using paired *t*-tests and determination coefficient (R^2) analysis (Amiri and Rezaei, 2010). The determination coefficient (R^2), which is defined as the squared value of the Pearson correlation coefficient, ranges from 0 to 1 (Raes et al., 2012a). It is clear that R^2 values close to 1 indicates less error variance, and values greater than 0.5 are commonly deemed acceptable in watershed scales (Vara Prasad et al., 2005). However, there are not any significant differences between the observed and simulated values if the P-value from the paired *t*-test is greater than 0.05 (Amiri and Rezaei, 2010).

2.3. Uncertainty of GCMs by applying ensemble means

The first step involved taking monthly temperature and precipitation data for the baseline (1985–2005) and future (2020–2039) periods

Table 3
Global Climate Models from IPCC, AR4 incorporated into the LARS-WG stochastic weather generator version 5.5.

Center	Model	Model acronym	Spatial Resolution	Emission Scenario
Australia's Commonwealth Scientific and Industrial Research Organization	CSIRO-MK3.0	CSMK3	1.9° × 1.9°	A1B, A2, B1
Canadian Centre for Climate Modelling and Analysis	CGCM33.1 (T47)	CGMR	2.8° × 2.8°	A1B, A2, B1
Bjerknes Centre for Climate Research	BCM2.0	BCM2	1.9° × 1.9°	A1B, A2, B1
Institute for Numerical Mathematics	INM-CM3.0	INCM3	4° × 5°	A1B, A2, B1
Goddard Institute for Space Studies	GISS-AOM	GIAOM	3° × 4°	A1B, B1

Table 4
Global climate models from IPCC AR5 incorporated into the LARS-WG stochastic weather generator version 5.5.

Center	Model	Model acronym	Spatial Resolution	RCP
Centre National de Recherches Meteorologiques, Meteo-France	CNRM-CM5	CNRM-CERFACS	1.40° × 1.40°	2.6, 8.5
Atmosphere and Ocean Research Institute (The University of Tokyo), National Institute for Environmental Studies and Japan Agency for Marine-Earth Science and Technology	MIROC-ESM	MIROC	2.79° × 2.81°	2.6, 8.5
Max-Planck Institute for Meteorology	MPI-ESM-LR	MPI-M	1.86° × 1.875°	2.6, 8.5
NASA/GISS (Goddard Institute for Space Studies) USA	GISS-E2-H	NASA-GISS	2.5° × 2°	2.6, 8.5
EC-EARTH consortium published at Irish Centre for High-End Computing Netherlands/Ireland	EC-EARTH	ICHEC	1.12° × 1.125°	2.6, 8.5
Meteorological Research Institute Japan	MRI-CGCM3	MRI	1.12° × 1.125°	2.6, 8.5
National Center for Atmospheric Research USA	CESM1 (WACCM)	NCAR NSF-DOE-NCAR	1.88° × 2.50°	2.6, 8.5

from the IPCC website (DDC: http://www.ipcc-data.org/). Different GCMs and emission scenarios that were selected in this study are shown in Tables 3 and 4. However, one of the most important uncertainties in climate change studies is uncertainty related to climate model output at regional scales. In this study, the weighting method of mean observed temperature-precipitation (MOTP) has been used to determine the uncertainty of climate models. This method weighted GCMs based on mean deviation between simulated and observed monthly values of temperature and precipitation in the baseline period. In other words, GCMs with greater weights can predict climatic values with more accuracy in the future.

The following equation, introduced by Massah Bavani (2006) as a weighting method, has been applied to climate change scenarios.

$$W_i = \frac{(1/\Delta T_{ij})}{\Sigma_{j=1}^{n}(1/\Delta T_{ij})} \quad (5)$$

where Wi is the weight of each model in month i, and ΔTij is the difference between average of temperature or precipitation simulated by AOGCM j in month i of the baseline period (1985–-2005) from the corresponding observed value (1985–2005).

To establish climate change scenarios, the following equations were applied between the average of 20 years from the future period (2020–2039) for each climate model and its simulated baseline period (1985–2005).

$$\Delta Ti = (\overline{T}_{GCM,fut,i} - \overline{T}_{GCM,base,i}) \quad (6)$$

$$\Delta Pi = (\overline{P}_{GCM,fut,i} - \overline{P}_{GCM,base,i}) \quad (7)$$

where ΔTi and ΔPi are climate change scenarios related to temperature and precipitation respectively for month i ($1 \le i \le 12$); $T_{GCM,fut,i}$ is the simulated future average temperature of 20 years derived from each climate model for month i; and $T_{GCM,base,i}$ is the simulated historical average temperature of 20 years derived from each climate model for month i. These variables have the same definition for precipitation.

To generate ensemble means, Eq. (8) is applied to LARS-WG scenario files within different GCMs and emission scenarios including B1, A1B, A2, RCP2.6, and RCP8.5 (Tables 3 and 4).

$$E = \sum_{i=1}^{n} Ti, j \times Wi, j \quad (8)$$

where Ti, j is taken from Eqs. (6) or (7), Wi,j is taken from Eq. (5), and n is the number of climate models.

2.4. LARS-WG model

Since the outputs provided by GCMs are too coarse in resolution, LARS-WG was used for the downscaling and generation of the climatic variables (Semenov and Barrow, 2002).

First, the determination of statistical characteristics was conducted, which is defined as model calibration (SITE ANALYSIS) using the observed daily weather data as a baseline period. The second step is model validation (QTEST), which describes the model performance. Moreover, those climatic variables that were used in the model calibration process are used for the generation of synthetic weather data, considering statistical characteristics to determine whether significant differences exist between the observed and synthetic weather data. Some statistical tests such as the Kolmogorov–Smirnov test and Student's *t*-test evaluate the differences between the distributions and mean values of the parameters derived from observed weather data and synthetic data. The last step is generation of daily climate variables, including minimum temperature, maximum temperature, and precipitation based on scenario files previously made by Eq. (8) by adjusting the Δ-changes for the future period.

2.5. Future yield, biomass, and comparison of treatments

For each emission scenario with different CO_2 rates, weighted multimodel ensemble means of temperature and precipitation for the years 2020–2039 were applied to the AquaCrop model to predict the yield and biomass for four varieties and three irrigation levels. Subsequently, the annual averaged values of yield and biomass for the future period 2020–2039 (2030s) under five emission scenarios were compared to the corresponding values of the historical period (1985–2010). Finally, stress tolerance (TOL) = $Y_p - Y_s$ (Rosielle and Hamblin, 1981) was applied to determine the most drought tolerant cultivars, where Y_p is without stress yield (control) and Y_s is the stress yield of a given cultivar. The cultivars with low values for this index are more stable under drought conditions.

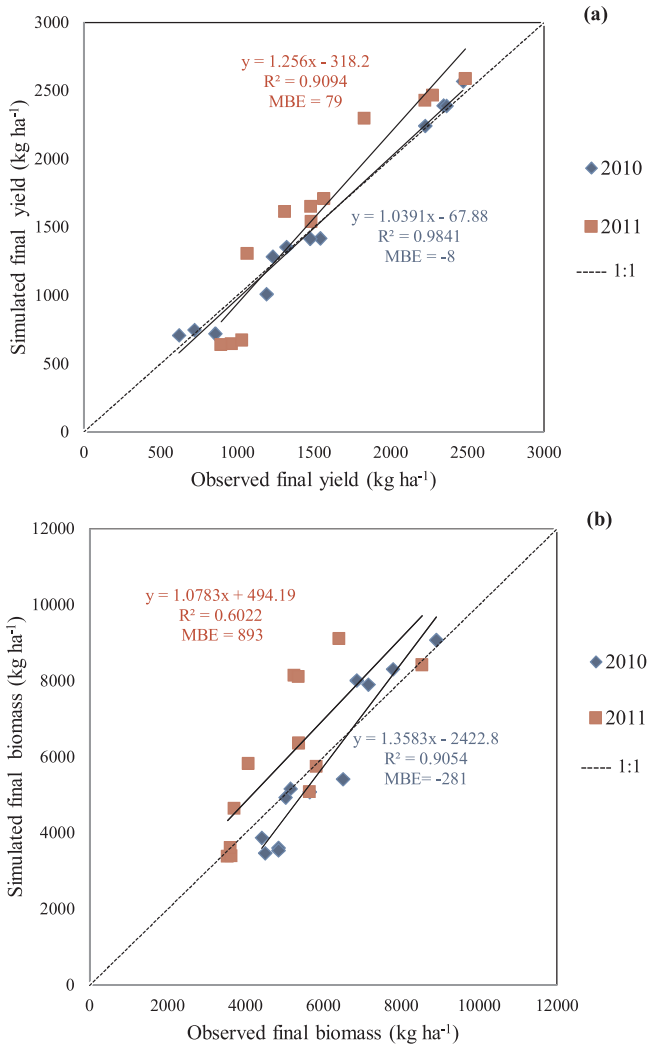

Fig. 1. Regression model between simulated versus observed (a) final yield and (b) biomass. The dotted line is 1:1.

3. Results

3.1. Model calibration and validation

The linear regression model between observed and simulated values of final yield and biomass is shown in Fig. 1a and b. The results indicated that slopes of regression were close to 1 and intercept values are relatively small. The correlation coefficients show that simulated and observed values were significantly correlated. The results of MBE showed that the model underestimated yield and biomass in 2010, whereas yield and biomass were overestimated in 2011.

The results of statistical analysis between model output and the observed data for all irrigation treatments and four soybean varieties in the calibration year 2010 are shown in Table 5. The model prediction accuracy pertaining to grain yield and biomass was evaluated by the following statistical indices: a root mean square error normalized (RMSEn) value of 6% for yield and 14% for biomass, paired *t*-test values of 0.49 for yield and 0.35 for biomass, and R^2 value of 0.98 for yield and 0.91 for biomass. The RMSEn values demonstrate that the model has excellent performance for yield and good performance for biomass. The paired *t*-tests did not recover any significant differences between the observed and simulated values of yield or biomass.

The results of statistical analysis between model output and the observed data for all irrigation treatments and four soybean varieties in the validation year 2011 are shown in Table 6. The model prediction accuracy pertaining to grain yield and biomass was evaluated by the following statistical indices: root mean square error normalized (RMSEn) values of 17% for yield and 30% for biomass, paired *t*-test values of 0.37 for yield and 0.12 for biomass, and R^2 values of 0.91 for yield and 0.60 for biomass. The RMSEn values demonstrate that the model has good performance for yield and fair performance for biomass. The paired *t*-tests did not recover any significant differences between the observed and simulated values of yield or biomass.

However, the results from observed and simulated data showed that water stress reduced yield and biomass, which is in agreement with the results of Ruttanaprasert et al. (2016), Montoya et al. (2016) and Tan et al. (2018). Although the AquaCrop model is a good choice for predicting yield and biomass, prediction errors for some treatments showed that AquaCrop performed better for less water stressed treatments, which is in agreement with results from Razzaghi et al. (2017).

Table 5
Evaluation results of grain yield and biomass in four soybean varieties under different irrigation levels in the calibration year of 2010.

	Yield (kg ha^{-1})		Biomass (kg ha^{-1})	
	Obs	Sim	Obs	Sim
Mean	1530	1522	5979	5698
SD	640	671	1387	1980
Min	621	710	4430	3469
Max	2473	2570	8907	9077
N	12		12	
MBE	−8		−281	
R^2	0.98		0.91	
P(t)	0.49*		0.35*	
RMSE	89		835	
RMSEn (%)	6		14	

Notes: The mean, standard deviation of population (SD), minimum, and maximum observed (OBS) and simulated (SIM) values are represented. Statistical analysis results are also shown: number of observations (N), mean bias error (MBE), correlation coefficient between simulated and observed values (r), P-value from the paired *t*-test [P (t)], absolute root mean square error (RMSE), normalized root mean square error (RMSEn), (*) means that simulated and observed values are the same at a 95% confidence level.

Table 6
Evaluation results of grain yield and biomass in four soybean varieties under different irrigation levels in the validation year of 2011.

	Yield (kg ha^{-1})		Biomass (kg ha^{-1})	
	Obs	Sim	Obs	Sim
Mean	1551	1630	5090	5983
SD	523	689	1421	1975
Min	896	639	3552	3382
Max	2488	2589	8548	9105
N	12		12	
MBE	79		893	
R^2	0.91		0.60	
P(t)	0.37*		0.12*	
RMSE	259		1537	
RMSEn(%)	17		30	

Notes: The mean, standard deviation of population (SD), minimum, and maximum observed (OBS) and simulated (SIM) values are represented. Statistical analysis results are also shown: number of observations (N), mean bias error (MBE), correlation coefficient between simulated and observed values (r), P-value from the paired t-test [P (t)], absolute root mean square error (RMSE), normalized root mean square error (RMSEn), (*) means that simulated and observed values are the same at a 95% confidence level.

3.2. LARS-WG

According to the results of model validation (QTEST), a statistical

Table 7
Climatic variables over the soybean growing season for the historical period (1985–2010) and the GCM outputs centered on 2030 s under different emission scenarios.

Period	Min-Temp (°C)	Max-Temp (°C)	Precipitation (mm)	CO_2 (ppm)
1985–2010	16.05	30.90	20.91	336.2
2030 s (RCP2.6)	**16.66**	**31.38**	26.52	428.6
2030 s (RCP8.5)	**17.41**	**31.86**	33.97	448.2
2030 s (B1)	16.74	31.71	**21.59**	437.3
2030 s (A1B)	16.87	31.82	**34.52**	**421.7**
2030 s (A2)	16.94	31.82	25.25	**452.7**

The bold values represent minimum and maximum values of projected climatic variables through five emission scenarios.

comparison was carried out between parameters derived from the observed weather data and synthetic weather data. Semenov and Barrow (2002) suggested that p-values less than 0.01 represent significant differences between the observed and simulated climatic variables. The p-values from the *t*-tests for all months and variables did not support significant differences between the means of the observed and predicted data. The Kolmogorov-Smirnov (K-S) test measured testing equality of the distributions of daily rainfall and temperature. When the p-value is greater than 0.01, the two datasets could have come from the same distribution. The p-values resulting from the Kolmogorov–Smirnov test were greater than 0.01 for the majority of the months. The only variable with a very low p-value was precipitation for September, which means that the semi-empirical distribution (SED) was not able to correctly reproduce the shape of the observed probability distributions due to heterogeneous distribution of precipitation in September. However, in general, the high p-values demonstrated excellent performance of LARS-WG for downscaling and generating daily climatic variables.

Comparisons between the changes of GCMs output under different emission scenarios, RCPs and the historical period over five significant growing months (July–October) are shown in Table 7. The findings showed that during the growing season means of minimum and maximum temperature, monthly precipitation, and annual CO_2 rate for the future 2030 s will be increased compared to their corresponding values in the historical period (1985–2010). In addition, the lowest and highest increases in future temperature were projected respectively by RCP2.6 and RCP8.5, whereas the lowest and highest increases in precipitation were projected respectively by B1 and A1B. The lowest and highest increase of future CO_2 rates were projected by A1B and A2, respectively.

3.3. Future yield and biomass

The averages of annual yields for the historical (1985–2010) and future (2030s) periods under the AR4 and AR5 emission scenarios are shown in Fig. 2. The averaged future yield within all emission scenarios under the control treatment showed that L17 had the greatest increase, followed by M7, W*H and M9, in that order. However, the predicted yield under mild water stress showed that M7 had the greatest increase, followed by L17, W*H and M9, in that order. Moreover, the predicted yield under severe water stress showed that M7 had the greatest increase, followed by L17, M9 and W*H, in that order. Based on stress tolerance (TOL), the most drought tolerant cultivar under mild water stress was M9, followed by M7, W*H and L17, sequentially, in all emission scenarios, RCP, and the historical period. However, the most tolerant cultivar under severe water stress was M7, followed by M9, W*H and L17, sequentially, in all emission scenarios, RCP, and the historical period.

The averages of annual biomass for the historical (1985–2010) and future (2030s) periods under the AR4 and AR5 emission scenarios are shown in Fig. 3. The averaged future biomass within all emission scenarios under the control treatment showed that L17 had the greatest increase, followed by W*H, M9 and M7, in that order. However, the predicted biomass under mild water stress showed that L17 exhibited the greatest increase, followed by M7, W*H and M9, in that order. The predicted biomass under severe water stress showed that M7 had the greatest increase, followed by M9, L17 and W*H, in that order.

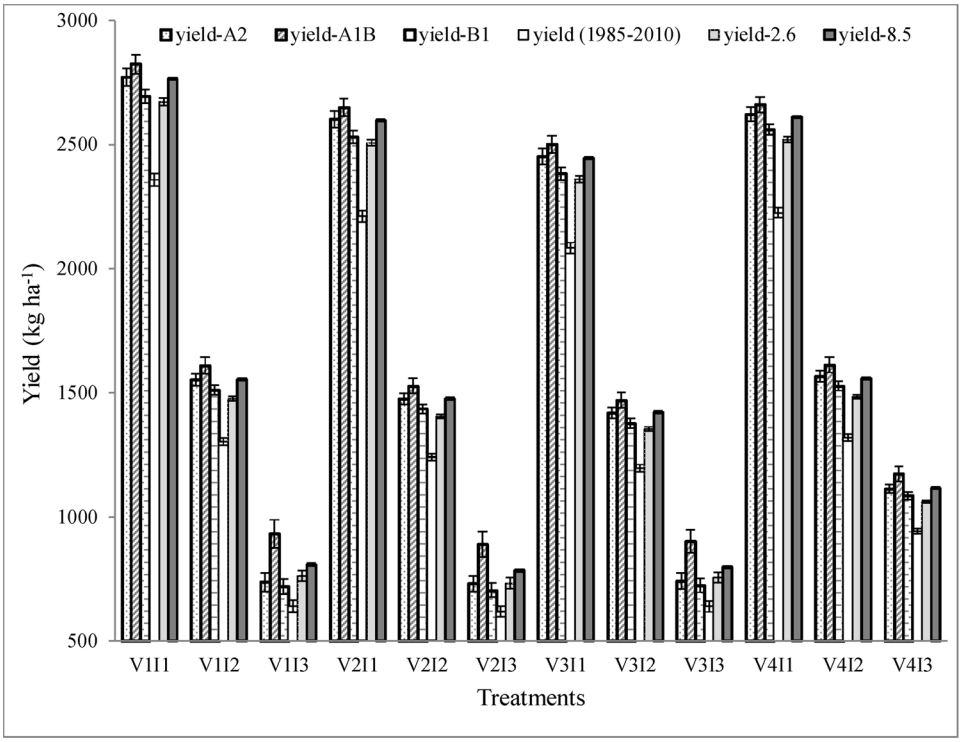

Fig. 2. Yield of different treatments in the historical period and predicted future period 2030 s under the AR4 and AR5 emission scenarios; the vertical bars represent the standard error of twenty years.

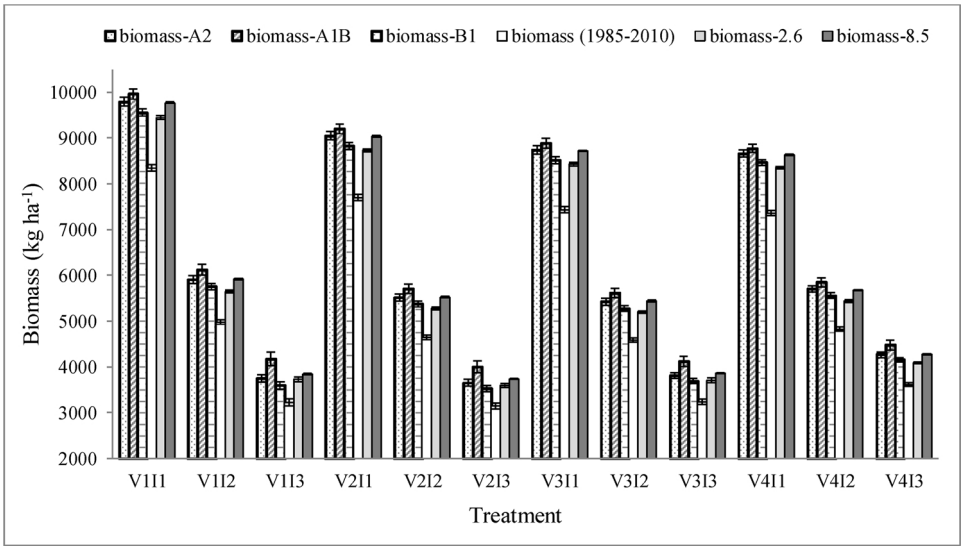

Fig. 3. Biomass of different treatments in the historical period and predicted future period 2030 s under the AR4 and AR5 emission scenarios; the vertical bars represent the standard error of twenty years.

Table 8
Correlation between climatic variables and averaged yield and biomass of four varieties under different irrigation levels.

Averaged yield and biomass of four varieties	Min-Temp	Max-Temp	Precipitation	CO_2
Yield without water stress (I1)	0.853*	0.960**	0.678	0.882*
Yield mild water stress (I2)	0.836*	0.962**	0.709	0.835*
Yield severe water stress (I3)	0.683	0.775	0.880*	0.542
Biomass without water stress (I1)	0.855*	0.961**	0.667	0.890*
Biomass mild water stress (I2)	0.841*	0.961**	0.710	0.842*
Biomass severe water stress (I3)	0.765	0.874*	0.819*	0.698

N = 6.
* Correlation is significant at the 0.05 level (2-tailed).
** Correlation is significant at the 0.01 level (2-tailed).

3.4. Impact assessment of climatic variables on soybean production

A Pearson correlation was conducted in SPSS for finding the probable relation between climatic variables (Table 7) and averaged final yield and biomass of all varieties under three irrigation levels. The correlation test (Table 8) showed that the final yield without water stress and with mild water stress were significantly correlated with maximum temperature at the 99% confidence level, minimum temperature and CO_2 at the 95% confidence level, while under severe water stress, the yield was significantly correlated to precipitation only at the 95% confidence level. This indicates that precipitation significantly affects final yield more than the other climatic variables do due to severe water shortages during the crop growth period.

According to Fig. 2, the greatest increase in yield was predicted under A1B, followed by RCP8.5, A2, B1, and RCP2.6, in descending order. On the other hand, based on Table 8, maximum temperature was highly correlated with yield under control and mild water stress, which was in agreement with the finding in Table 7 that maximum temperature increased under RCP8.5 followed by A1B, A2, B1, RCP2.6. However, the results from increasing mean maximum monthly temperature during the seed filling months in the 2030 s compared to those of the historical period were in agreement with Isoda et al. (2010), which declared that global warming will likely continue to benefit the soybean yield of the study area located in Northeast China for a few decades.

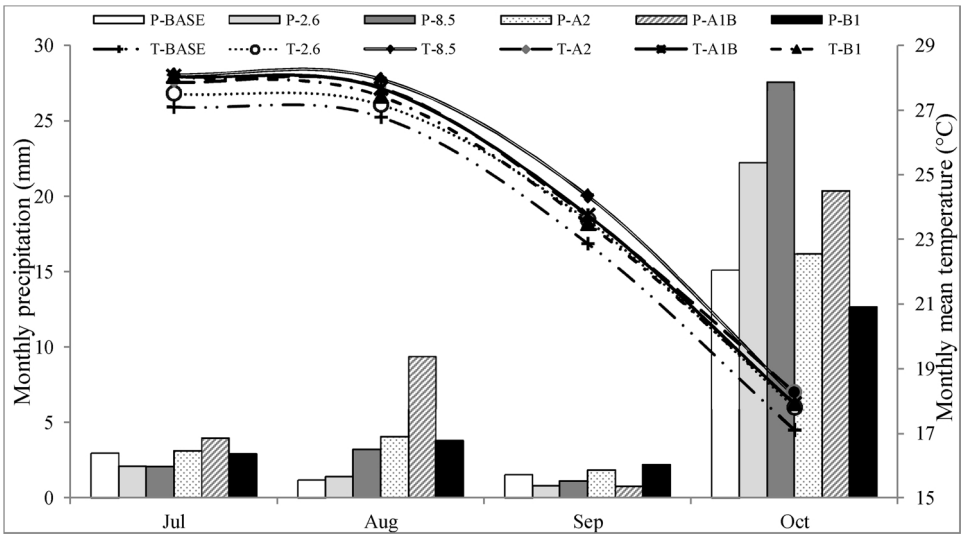

Fig. 4. Monthly precipitation (mm) and monthly mean temperature (°C) for the historical period (1985–2010) and future period 2030 s during soybean growing season.

Table 9
Monthly mean temperature and monthly averaged in reproductive development stage and the entire growing season.

Mean temperature (°C)	July	August	September	October	Reproductive stage (Aug–Sep)	Growing season (July–Oct)
1985–2010	27.10	26.80	22.85	17.15	24.83	23.48
2030 s (RCP2.6)	27.52	27.18	23.59	17.80	25.38	24.02
2030 s (RCP8.5)	28.09	27.96	24.35	18.15	26.15	24.64
2030 s (B1)	28.05	27.43	23.50	17.92	25.47	24.23
2030 s (A1B)	28.04	27.67	23.75	17.91	25.71	24.34
2030 s (A2)	27.86	27.71	23.70	18.27	25.70	24.38

The results from Table 8 also showed that biomass is statistically significant to maximum temperature at 99% confidence level for control treatments, followed by CO_2 and minimum temperature at the 95% confidence level. However, under mild water stress, biomass is statistically significantly correlated with maximum temperature at the 99% confidence level, followed by CO_2 and minimum temperature at the 95% confidence level, whereas under severe water stress, biomass is statistically significantly correlated with maximum temperature and precipitation at the 95% confidence level. According to Fig. 3, the greatest increase in biomass was predicted under A1B, followed by RCP8.5, A2, B1, and RCP2.6, in descending order. However, based on Table 8, maximum temperature was highly correlated with biomass under control and mild water stress, which was in agreement with Table 7, which showed that maximum temperature increased under RCP8.5, followed by A1B, A2, B1, RCP2.6. However, in the severe water stress treatment, the maximum temperature followed by precipitation both influence biomass, which was in agreement with the results of Table 7.

The monthly precipitation and monthly mean temperature for the historical (1985–2010) and future (2030s) period during the soybean growing season are shown in Fig. 4. Although under the A1 B scenario, CO_2 increases less than it does under the other emission scenarios (Table 7), it predicts the highest levels of yield and biomass in the 2030 s compared to those of the other scenarios (Figs. 2 and 3). This reason could be due to precipitation increases during the flowering and initial phase of seed filling stages in August (Fig. 4), which can compensate for water shortage in this sensitive growing month.

The monthly mean temperatures in the soybean reproductive development stage (August to September) and the entire growing season (July to October) for the historical and projected periods are shown in Table 9, which demonstrate the optimum temperature in the future. Studies have shown that the reproductive phase, including the flowering and seed filling periods, are the most sensitive growth stage of crops to heat stress (Singh et al., 2010; Teixeira et al., 2013). Gibson and Mullen (1996) reported that the optimum average temperature for the reproductive growth stage is 29 °C, and at higher temperatures (e.g., 37 °C), the soybean yield will significantly decrease. In addition, Grimm et al. (1994) reported that the optimum temperature for the reproductive growth period varies between 25.0 and 29.0 °C.

Tacarindua et al. (2013) indicated that yield decreased for treatments with higher mean temperature in the growing season. The mean temperature varied within the range of 25.7–31.1 °C for different treatments. However, since the highest yield occurred for the treatment with 25.7 °C, this value could be considered as the optimum mean temperature during the growing season. Choi et al. (2016) found that the optimum growing season (VE-R7) temperatures for seed yield were 25.0 and 26.4 °C for two different cultivars. According to Table 9 and Fig. 4 in this study, temperatures below the optimum level appear to have occurred in the historical period. In other words, the mean temperature values for the reproductive stage and the entire growing season (Table 9) show that under future climate change scenarios, the temperature will more closely reflect the optimum thresholds, which might be higher than 25.0 °C for increasing final yield. Moreover, based on projected climate change models, precipitation will be increased under all emission scenarios in August (Fig. 4), when soybeans are passing the reproductive stage. On the other hand, elevated CO_2 induced higher yields (Nakamoto et al., 2004) and biomass (Matsunami et al., 2009) during the growing period, which is in line with the results of this study. In fact, CO_2 allows partial stomatal closure, which reduces transpiration rate and consequently increases water use efficiency (Boote, 2011). Therefore, increased precipitation and CO_2 rates in the future will offset the deleterious effects of heat stress, particularly when irrigation declines and crops are coping with water stress.

4. Conclusions

It is clear that changes in temperature, rainfall, and CO_2 rate in the future (2030s) will influence soybean growth and the final grain yield. However, studies regarding these variables in Iran are limited, and most investigations have focused on impacts of planting date, drought stress, irrigation regimes, and variety on growth and yield of soybean. Moreover, the weighted multi-model ensemble means method was able to model the uncertainty of climate models through the contribution of LARS-WG with very good performance for the downscaling and generation of climatic variables for the future 2030s.

According to stress tolerance (TOL), short-growing cultivars are the most tolerant cultivars under mild (M7) and severe water stress (M9). The M7, L17, W*H, and M9 varieties showed the highest to lowest increases in the means of the yield over all three irrigation levels under projected climate change, whereas L17, M7, W*H, and M9 showed the highest to lowest increases in the means of the biomass over all three irrigation levels under projected climate change. However, selecting the best varieties in each cultivation year should be considered with other existing limitations such as irrigation and field management, soil, and climatic conditions.

Differences in crop management and agricultural practices may also have contributed to variations in yield and biomass. However, for the prediction of future yield and biomass, these factors are considered similar to the calibration year. In this research, under projected climate change, increase of maximum temperature had a significantly positive effect on yield and biomass with the exception of yield under severe water stress conditions, in which precipitation had the greatest influence on final yield. It is also clear that yield and biomass increased for all treatments in the 2030s. However, heat stress during the flowering stage can decrease yield significantly. Under heat stress conditions, the cultivar type plays an important role for preserving a greater number of flowers and seeds by allocation of more assimilated materials to reproductive organs and avoidance of heat stress by shortening the vegetative period and accelerating flowering. Therefore, rainfall, temperature, and CO_2 rate during the flowering and yield formation stages should be taken into account for yield prediction.

Since the study area is located in a cold semi-arid climate, it may be concluded that soybean will reach optimal temperature for yield formation during the flowering and seed filling periods due to future increases in temperature.

Disclosure statement

The authors declare no conflicts of interest.

Acknowledgements

The authors acknowledge the cooperation of the Karaj Seed and Plant Improvement Institute, Department of Oil Seed Crops. This project was funded by Universiti Putra Malaysia (grant vot no. 9573700). The support from all the UPM staff is greatly appreciated.

References

Alexandrov, V., Genev, M., 2003. Climate Variability and Change Impact on Water Resources in Bulgaria. European Water. pp. 20–25 e-bulletin of EWRA 1.
Amiri, E., Rezaei, M., 2010. Evaluation of water–nitrogen schemes for rice in Iran, using ORYZA2000 model. Commun. Soil Sci. Plant Anal. 41, 2459–2477.
Amiri, E., Ahmadzadeh Araji, H., Wayayok, A., Rezaei, M., 2015. Simulation of rice yield under water and salinity stress in rasht area using aquacrop model. Jurnal Teknologi 76.
Andarzian, B., Bannayan, M., Steduto, P., Mazraeh, H., Barati, M., Barati, M., Rahnama, A., 2011. Validation and testing of the AquaCrop model under full and deficit irrigated wheat production in Iran. Agric. Water Manage. 100, 1–8.
Araya, A., Keesstra, S., Stroosnijder, L., 2010. Simulating yield response to water of Teff (*Eragrostis tef*) with FAO's AquaCrop model. Field Crops Res. 116, 196–204.
Bannayan, M., Crout, N., Hoogenboom, G., 2003. Application of the CERES-Wheat model for within-season prediction of winter wheat yield in the United Kingdom. Agron. J. 95, 114–125.
Boote, K.J., 2011. Improving soybean cultivars for adaptation to climate change and climate variability. Crop Adaptation to Climate Change. pp. 370–395.
Brouyère, S., Dassargues, A., 2004. Spatially distributed, physically-based modelling for simulating the impact of climate change on groundwater reserves. Hydrology: Science and Practice for the 21 st Century.
Choi, D.-H., Ban, H.-Y., Seo, B.-S., Lee, K.-J., Lee, B.-W., 2016. Phenology and seed yield performance of determinate soybean cultivars grown at elevated temperatures in a temperate region. PLoS One 11, e0165977.
Farahani, H.J., Izzi, G., Oweis, T.Y., 2009. Parameterization and evaluation of the AquaCrop model for full and deficit irrigated cotton. Agron. J. 101, 469–476.
Fowler, H., Kilsby, C., Webb, B., Arnell, N., Onof, C., MacIntyre, N., Gurney, R., Kirby, C., 2004. Future increase in UK water resource drought projected by a regional climate model, Hydrology: science and practice for the 21st century. In: Proceedings of the British Hydrological Society International Conference. Imperial College, London, July 2004. British Hydrological Society. pp. 15–21.
García-Vila, M., Fereres, E., 2012. Combining the simulation crop model AquaCrop with an economic model for the optimization of irrigation management at farm level. Eur. J. Agron. 36, 21–31.
Gellens, D., Roulin, E., 1998. Streamflow response of Belgian catchments to IPCC climate change scenarios. J. Hydrol. 210, 242–258.
Gibson, L.R., Mullen, R.E., 1996. Influence of day and night temperature on soybean seed yield. Crop Sci. 36, 98–104.
Grimm, S.S., Jones, J.W., Boote, K.J., Herzog, D.C., 1994. Modeling the occurrence of reproductive stages after flowering for four soybean cultivars. Agron. J. 86, 31–38.
Heidariniya, M., Naseri, A.A., Boroumandnasab, S., Moshkabadi, B.S., Nasrolahi, A., 2012. Evalution of AquaCrop Model Application in Irrigation Management of Cotton.
Hussein, F., Janat, M., Yakoub, A., 2011. Simulating cotton yield response to deficit irrigation with the FAO AquaCrop model. Span. J. Agric. Res. 9, 1319–1330.
IPCC-TGICA, 2007. General Guidelines on the Use of Scenario Data for Climate Impact and Adaptation Assessment. Version 2. Prepared by T.R. Carter on behalf of the Intergovernmental Panel on Climate Change, Task Group on Data and Scenario Support for Impact and Climate Assessment, 66pp.
Iqbal, M.A., Shen, Y., Stricevic, R., Pei, H., Sun, H., Amiri, E., Penas, A., del Rio, S., 2014. Evaluation of the FAO AquaCrop model for winter wheat on the North China Plain under deficit irrigation from field experiment to regional yield simulation. Agric. Water Manage. 135, 61–72.
Isoda, A., Mao, H., Li, Z., Wang, P., 2010. Growth of high-yielding soybeans and its relation to air temperature in Xinjiang, China. Plant Prod. Sci. 13, 209–217.
Jacovides, C.P., Kontoyiannis, H., 1995. Statistical procedures for the evaluation of evapotranspiration computing models. Agric. Water Manage. 27, 365–371.
Kamga, F.M., 2001. Impact of greenhouse gas induced climate change on the runoff of the Upper Benue River (Cameroon). J. Hydrol. 252, 145–156.
Knutti, R., Sedláček, J., 2012. Robustness and uncertainties in the new CMIP5 climate model projections. Nat. Clim. Change 3, 369.
Massah Bavani, A., 2006. Risk Assessment of Climate Change and Its Impact on Water Resources, A Case Study in Zayandeh Rud Basin. Tarbiat Modares University p. 218.
Masuda, T., Goldsmith, P.D., 2009. World soybean production: area harvested, yield, and long-term projections. Int. Food Agribus. Manage. Rev. 12, 143–162.
Matsunami, T., Otera, M., Amemiya, S., Kokubun, M., Okada, M., 2009. Effect of CO2 concentration, temperature and N fertilization on biomass production of soybean genotypes differing in N fixation capacity. Plant Prod. Sci. 12, 156–167.
Minville, M., Brissette, F., Leconte, R., 2008. Uncertainty of the impact of climate change on the hydrology of a nordic watershed. J. Hydrol. 358, 70–83.
Montoya, F., Camargo, D., Ortega, J.F., Córcoles, J.I., Domínguez, A., 2016. Evaluation of Aquacrop model for a potato crop under different irrigation conditions. Agric. Water Manage. 164, 267–280.
Mustafa, S.M.T., Vanuytrecht, E., Huysmans, M., 2017. Combined deficit irrigation and soil fertility management on different soil textures to improve wheat yield in drought-prone Bangladesh. Agric. Water Manage. 191, 124–137.
Nakamoto, H., Zheng, S.-H., Tanaka, K., Yamazaki, A., Furuya, T., Iwaya-Inoue, M., Fukuyama, M., 2004. Effects of carbon dioxide enrichment during different growth periods on flowering, pod set and seed yield in soybean. Plant Prod. Sci. 7, 11–15.
Prudhomme, C., Davies, H., 2007. Comparison of Different Sources of Uncertainty in Climate Change Impact Studies in Great Britain. pp. 183–190 Technical Document in Hydrology-UNESCO Paris 80.
Raes, D., Steduto, P., Hsiao, T.C., Fereres, E., 2009a. AquaCrop—The FAO Crop Model to Simulate Yield Response to Water FAO Land and Water Division. FAO, Rome.
Raes, D., Steduto, P., Hsiao, T.C., Fereres, E., 2009b. AquaCrop the FAO crop model to simulate yield response to water: II: main algorithms and software description. Agron. J. 101, 438–447.
Raes, D., Steduto, P., Hsiao, T.C., Fereres, E., 2012a. Land and Water Division. FAO, Rome, Italy.
Raes, D., Steduto, P., Hsiao, T.C., Fereres, E., 2012b. Reference Manual AquaCrop 4.0. FAO, Rome.
Randall, D.A., Wood, R.A., Bony, S., Colman, R., Fichefet, T., Fyfe, J., Kattsov, V., Pitman, A., Shukla, J., Srinivasan, J., Stouffer, R.J., Sumi, A., Taylor, A.K.E., 2007. Cilmate models and their evaluation. In: Solomon, S., Qin, D., Manning, M., Chen, Z., Marquis, M., Averyt, K.B., Tignor, M., Miller, H.L. (Eds.), Climate Change 2007: The Physical Science Basis. Contribution of Working Group I to the Fourth Assessment Report of the Intergovernmental Panel on Climate Change. Cambridge University Press Cambridge, United Kingdom and New York, NY, USA, pp. 590–662.
Raziei, T., Pereira, L.S., 2013. Estimation of ET o with Hargreaves–Samani and FAO-PM temperature methods for a wide range of climates in Iran. Agric. Water Manage. 121, 1–18.
Razzaghi, F., Zhou, Z., Andersen, M.N., Plauborg, F., 2017. Simulation of potato yield in temperate condition by the AquaCrop model. Agric. Water Manage. 191, 113–123.
Rosielle, A., Hamblin, J., 1981. Theoretical aspects of selection for yield in stress and non-stress environment. Crop Sci. 21, 943–946.
Ruosteenoja, K., Carter, T.R., Jylhä, K., Tuomenvirta, H., 2003. Future Climate in World Regions: an Intercomparison of Model-based Projections for the New IPCC Emissions Scenarios. Finnish Environment Institute, Helsinki.
Ruttanaprasert, R., Jogloy, S., Vorasoot, N., Kesmala, T., Kanwar, R.S., Holbrook, C.C., Patanothai, A., 2016. Effects of water stress on total biomass, tuber yield, harvest index and water use efficiency in Jerusalem artichoke. Agric. Water Manage. 166, 130–138.
Salemi, H., Soom, M.A.M., Lee, T.S., Mousavi, S.F., Ganji, A., Yusoff, M.K., 2011. Application of AquaCrop model in deficit irrigation management of winter wheat in arid region. Afr. J. Agric. Res. 6, 2204–2215.
Semenov, M.A., Barrow, E.M., 2002. LARS-WG: A Stochastic Weather Generator for Use in Climate Impact Studies, Version 3.0, User Manual.
Shrestha, N., Raes, D., Vanuytrecht, E., Sah, S.K., 2013. Cereal yield stabilization in Terai (Nepal) by water and soil fertility management modeling. Agric. Water Manage. 122, 53–62.
Singh, S.K., Kakani, V.G., Surabhi, G.-K., Reddy, K.R., 2010. Cowpea (Vigna unguiculata [L.] Walp.) genotypes response to multiple abiotic stresses. J. Photochem. Photobiol. B 100, 135–146.
Steduto, P., Raes, D., Hsiao, T.C., Fereres, E., Heng, L.K., Howell, T.A., Evett, S.R., Rojas-Lara, B.A., Farahani, H.J., Izzi, G., 2009. Concepts and Applications of AquaCrop: The FAO Crop Water Productivity Model, Crop Modeling and Decision Support. Springer, pp. 175–191.
Tabari, H., 2010. Evaluation of reference crop evapotranspiration equations in various climates. Water Resour. Manage. 24, 2311–2337.
Tacarindua, C.R.P., Shiraiwa, T., Homma, K., Kumagai, E., Sameshima, R., 2013. The effects of increased temperature on crop growth and yield of soybean grown in a temperature gradient chamber. Field Crops Res. 154, 74–81.
Tan, S., Wang, Q., Zhang, J., Chen, Y., Shan, Y., Xu, D., 2018. Performance of AquaCrop model for cotton growth simulation under film-mulched drip irrigation in southern Xinjiang, China. Agric. Water Manage. 196, 99–113.
Tavakoli, A.R., Moghadam, M.M., Sepaskhah, A.R., 2015. Evaluation of the AquaCrop model for barley production under deficit irrigation and rainfed condition in Iran. Agric. Water Manage. 161, 136–146.
Teixeira, E.I., Fischer, G., van Velthuizen, H., Walter, C., Ewert, F., 2013. Global hot-spots of heat stress on agricultural crops due to climate change. Agric. Forest Meteorol. 170, 206–215.
Vara Prasad, P., Allen Jr, L., Boote, K., 2005. Crop responses to elevated carbon dioxide and interaction with temperature: grain legumes. J. Crop Improv. 13, 113–155.
Yang, C., Fraga, H., Ieperen, W.V., Santos, J.A., 2017. Assessment of irrigated maize yield response to climate change scenarios in Portugal. Agric. Water Manage. 184, 178–190.
Yates, D.N., Strzepek, K.M., 1998. Modeling the Nile basin under climatic change. J. Hydrol. Eng. 3, 98–108.
Yuan, M., Zhang, L., Gou, F., Su, Z., Spiertz, J., Van Der Werf, W., 2013. Assessment of crop growth and water productivity for five C 3 species in semi-arid Inner Mongolia. Agric. Water Manage. 122, 28–38.
van Vuuren, D.P., Edmonds, J., Kainuma, M., Riahi, K., Thomson, A., Hibbard, K., Hurtt, G.C., Kram, T., Krey, V., Lamarque, J.-F., Masui, T., Meinshausen, M., Nakicenovic, N., Smith, S.J., Rose, S.K., 2011. The representative concentration pathways: an overview. Clim. Change 109, 5.